ORIGINAL RESEARCH

Accelerated Fibrosis Progression of Diabetic Nephropathy From High Uric Acid's Activation of the ROS/NLRP3/SHP2 Pathway in Renal Tubular Epithelial Cells Under High Glucose Conditions

Ling Tian, BD; Qian Yu, BD; Li Zhang, BD; Jiwei Zhang, BD

ABSTRACT

Context • Elevated uric-acid levels in the blood are closely associated with hypertension, metabolic syndrome, diabetic nephropathy, cardiovascular diseases, and chronic kidney disease (CKD). A high-glucose diet promotes the accumulation of uric acid. Fibrosis commonly occurs in patients with late-stage type 1 or 2 diabetes and can lead to organ dysfunction

Objective • The study intended to investigate whether high uric acid under high glucose conditions can promote the fibrotic progression of diabetic nephropathy by activating the reactive oxygen species (ROS)/ "nod-like receptor (NLR) family pyrin domain containing 3" (NLRP3)/ "Src homology 2 (SH2) domain-containing protein tyrosine phosphatase-2" (SHP2) pathway, which can promote epithelial-mesenchymal transition (EMT) in renal tubular epithelial cells.

Design • The research team conducted an animal study.

Setting • The study took place at the Affiliated Hospital of Hebei University in Baoding, Hebei Province, China.

Animals • The animals were 14 healthy, male, C57BL/6J mice.

Outcome Measures • The research team: (1) using Masson's trichrome staining, examined the fibrosis of renal, tubular epithelial cells in the streptozotocin (STZ) modeling and the STZ modeling + uric-acid groups; (2) used Western Blot analysis to detect the protein expression of NLRP3, "nicotinamide-adenine dinucleotide phosphate (NADPH) oxidase 2" (NOX2), NOX4, alpha-smooth muscle actin (α-SMA), fibronectin 1 (FN-1), collagen-I, and mothers against decapentaplegic homolog 2/3 (SMAD2/3); (3) conducted in-vitro experiments by dividing transformed C3H mouse kidney-1 (TCMK-1) cells into different groups: STZ modeling group, STZ modeling + high-glucose group, STZ modeling + high-glucose + advanced glycation end (AGE) product group, STZ modeling+ high-glucose + AGE + uric-acid group, STZ modeling+ high glucose + SHP2 small interfering RNA (SiRNA) group, STZ modeling + high glucose + SHP2 SiRNA + AGE group, and STZ modeling+ high-glucose + SHP2 SiRNA + AGE + uric-acid group for Western Blot experiments; and (4) performed immunofluorescence, CCK-8, and transwell experiments on the seven groups of TCMK-1 cells with different treatments.

Results • The STZ modeling + uric acid group's levels of fibrosis was significantly higher than that of the STZ modeling group ($P < .01$). Additionally, the STZ modeling + uric acid groups' expression of α-SMA, FN-1, collagen-I, P-SMAD2, P-SMAD3, NLRP3, and reactive oxygen species (ROS), EMT, and SMAD-related proteins were significantly higher than those of the STZ modeling group ($P < .01$). The protein expression of SHP2, P-SMAD2, α-SMA, and FN-1 for the STZ modeling + high glucose + SHP2 SiRNA, the STZ modeling + high glucose + SHP2 SiRNA + AGE, and the STZ modeling + high glucose + SHP2 SiRNA + AGE + uric acid groups were significantly lower than those of the STZ modeling + high glucose, STZ modeling + high glucose + AGE, and the STZ modeling + high glucose + AGE + uric acid groups, respectively.

Immunofluorescence indicated that the STZ modeling+ high glucose + AGE + uric acid group had the highest relative fluorescence intensity, while the three groups treated with SHP2 SiRNA showed the least expression. The cell counting kit-8 (CCK-8) assay showed that STZ modeling group had less cell proliferation, STZ modeling + high sugar group had less cell proliferation than STZ modeling + high sugar +AGE group, STZ modeling + high sugar +AGE+ uric acid group had the highest cell proliferation, STZ modeling + high sugar +SHP2 SiRNA group and STZ modeling + high sugar +SHP2 SiRNA+AGE group and STZ modeling + high sugar +SHP2 SiRNA+AGE+ uric acid group showed the least number of cell proliferation. The results of the transwell cell migration assay were consistent with the CCK-8 assay.

Conclusions • In a high-glucose environment, high uric acid can promote the fibrotic progression of diabetic nephropathy by activating the ROS/NLRP3/SHP2 pathway, leading to mesenchymal transition between renal tubular epithelial cells. (*Altern Ther Health Med.* [E-pub ahead of print.])

Ling Tian, BD, Attending Physician; **Li Zhang**, BD, Attending Physician, Department of Nephrology; Key Laboratory of Bone Metabolism and Physiology in Chronic Kidney Disease of Hebei Province; Affiliated Hospital of Hebei University; Baoding; Hebei Province; China. **Qian Yu**, BD, Attending Physician, Department of Geriatrics; Affiliated Hospital of Hebei University; Baoding; Hebei Province; China. **Jiwei Zhang**, BD, Attending Physician, Department of Cardiovascular Medicine; Affiliated Hospital of Hebei University; Baoding; Hebei Province; China.

Corresponding author: Jiwei Zhang, BD
E-mail: 19931215144@163.com

INTRODUCTION

The main product in normal human urine is urea, with a small amount of uric acid that is the end product of purine metabolism, a trioxypurine that exhibits weak acidic properties. The oxidation of various purines generates uric acid in the urine.

An imbalance between the production and excretion of uric acid in the body can lead to elevated uric-acid levels in the blood. These are closely associated with hypertension, metabolic syndrome, diabetic nephropathy, and cardiovascular diseases and also can serve as an independent risk factor for the occurrence and progression of chronic kidney disease (CKD).[1]

Estimates that CKD affects 10-14% of the global population.[2] Renal fibrosis, characterized by excessive and

inappropriate deposition of extracellular matrix in various tissues,[3] can lead to scar formation and is a hallmark feature of progressive CKD. However, currently, no specific antifibrotic therapies exist for CKD.

Renal Fibrosis

Renal fibrosis manifests as tubular atrophy, interstitial chronic inflammation and fibrosis, glomerulosclerosis, and vascular rarefaction. The fibrotic niche is the site where organ fibrosis initiates, involving complex interactions between damaged parenchymal cells, such as tubular cells, and various nonparenchymal cell lineages—immune cells and stromal cells—that are present within the scarred area.

Currently, there is no effective medication available for fibrotic kidney disease. Most therapies can only delay the progression of the disease, highlighting the urgent need for innovative approaches to explore disease reversal or prevention. Although the mechanisms of renal fibrosis have become complex due to the involvement of various cell types, the use of single-cell technology (Single-cell layer assembly technology (LBL) can construct a 3D hypoxic microenvironment culture system. Compared with the traditional two-dimensional cell culture system, the three-dimensional cell culture system can better simulate the real and complex in vivo environment), With the help of this technology, many key questions have been explored, such as which renal tubules promote fibrosis, the origin of myofibroblasts, the involvement of immune cells, and how cells communicate with each other.[4] In this study, we aim to investigate the changes in renal tubular epithelial cells to explore the progression of fibrosis in diabetic kidney disease.

Diabetes

Hyperuricemia and its tubular damage have become a focus and important topic in kidney-disease research. A high-glucose diet promotes the accumulation of uric acid and the formation of kidney stones, a process exacerbated by dehydration and physiological acidification. Furthermore, van Dam et al's metabolomic analysis with humans found that dietary sugar intake can strongly influence purine levels.[5]

The incidence and mortality rates associated with diabetes are mainly due to potential debilitating complications, such as heart and kidney failure, hepatic dysfunction, retinopathy, and peripheral neuropathy. Fibrosis commonly occurs in patients with late-stage type 1 or 2 diabetes and can lead to organ dysfunction.[3]

High-glucose stimulation can: (1) trigger multiple fibrotic pathways; (2) induce reactive oxygen species (ROS) generation; (3) activate neurohumoral responses; (4) initiate growth factor cascades, such as those of transforming growth factor-beta (TGF-β)/ mothers against decapentaplegic homolog 3 (SMAD3) and of platelet-derived growth factor (PDGF); (5) induce pro-inflammatory cytokines and chemokines; (6) produce advanced glycation end (AGE) products; (7) stimulate the AGE-receptor for the AGEs (RAGE) axis; and (8) upregulate fibrotic matrix proteins.[6]

Diabetes and Fibrosis

Due to the widespread impact of diabetes-related fibrosis on several important organs including the kidneys, heart, and liver, strategies to alleviate fibrosis in diabetic patients are highly attractive because they could reduce organ dysfunction. Some measures can provide beneficial effects and can delay the progression of kidney or cardiovascular diseases in diabetic patients, such as optimal blood-glucose control or the protective effects of drugs such as angiotensin-converting enzyme inhibitors or statins. However, these are at least partially mediated through the attenuation of fibrosis.

Furthermore, using models of diabetic cardiomyopathy and kidney disease with early initiation of treatment with AGE crosslink breakers, Candido and Forbes found that the treatment could restore collagen solubility,[7] and Forbes et al found that it could improve functional parameters.[8] The formation of AGEs occurs through the direct reaction of methylglyoxal (MG) with lysine and arginine residues on proteins. MG is a reactive metabolite that primarily forms as a byproduct of glucose metabolism.[9]

When applied to mice in vitro or cultured cells in vivo, MG mimics the pathological changes typically associated with diabetes.[10,11] We found that in an MG-related diabetic environment, the receptor for AGES (RAGE)/ nuclear factor kappa B (NF-κB) axis drives the expression of SHP-2.

SHP2

Although the fibrotic signaling that diabetes activates shares common features in various tissues, certain organs, such as the heart, kidneys, and liver, can develop more pronounced and clinically significant fibrosis. AGEs can promote ROS activity, while uric-acid-crystal deposition can promote the "nod-like receptor (NLR) family pyrin domain containing 3" (NLRP3) inflammasome response, thereby activating the ROS/ NLRP3/ "Src homology 2 (SH2) domain-containing protein tyrosine phosphatase-2" (SHP2) pathway.

Epithelial-mesenchymal transition (EMT) is a form of cellular differentiation involved in development, fibrosis, and wound-healing processes.[12] Qu and Feng and Wright et al found that SHP2 plays a crucial role in cellular differentiation, suggesting its potential involvement in EMT regulation.[13,14] SHP2, a member of the nonreceptor, protein tyrosine phosphatase family, participates in various signaling pathways and activates the rat sarcoma (Ras)/ extracellular-signal-regulated kinase (ERK) signaling pathway primarily through epidermal growth factor (EGF) binding to EGF receptors.[15,16] This suggests a potential regulatory role for SHP2 in the EMT process,[17,18]

Current Study

The current study intended to investigate whether high uric acid under high glucose conditions can promote the fibrotic progression of diabetic nephropathy by activating the ROS/NLRP3/SHP2 pathway, which can promote epithelial-mesenchymal transition in renal tubular epithelial cells.

METHODS

Animals

The research team conducted an animal study, which took place at the Affiliated Hospital of Hebei University in Baoding, Hebei Province, China. The research team purchased 14 healthy, male, C57BL/6J mice from SCBS Biotechnology Co. LTD (Anyang City, China; SCXK(YU) 2020005). The team provided the mice with ad-libitum access to food and water and housed mice at a temperature of 23-25°C, with a humidity of 40%-60%. The animal experimental procedures were fully compliant with approved guidelines and ARRIVE guidelines.

Procedures

Materials. The research team purchased: (1) streptozotocin (STZ) solution from Shanghai Maokang Biotechnology Co., Ltd. (Shanghai, China; MS1601); (2) uric-acid crystals from AmyJet Scientific Co., Ltd. (Wuhan, China; MBS6021534), advanced glycation end-products (AGEs) from Bioss ANTIBODIES Co.,Ltd. (Beijing, China; bs-1158P); (3) 4% formaldehyde fixative, ethanol, xylene, hematoxylin staining solution, and fuchsin were purchased from Beijing BioLegend Technology Co., Ltd. (Beijing, China; YTB1299, GL0676, WH0015, YT911, YT870); (4) Masson's trichrome staining kit from Beyotime Co., Ltd (Shanghai, China; C0189S); (5) hydrochloric acid alcohol from Beyotime Co., Ltd (Shanghai, China; C0163L); (6) acetic acid from Nanjing Reagent Co., Ltd. (Nanjing, China; C0680265223; (7) neutral resin from Sangon Biotech Co., Ltd. (Shanghai, China; E675007-0100); microscope for microscopic examination and image-acquisition from OLYMPUS Co., Ltd. (Tokyo, Japan; BX63); (8) commercial kit for extraction of cellular total protein from Solarbio Technology Co., LTD. (Beijing, China; BC3710); (9) polyvinylidene fluoride (PVDF) from MERCK Co., LTD.(Beijing, China; 427152); (10) primary antibodies against alpha-smooth muscle actin (α-SMA) from Abbkine Co., LTD. (Wuhan, China; ABM0052), fibronectin 1 (FN-1) from Yeasen Biotechnology Co., LTD. (Shanghai, China; 40113ES03), collagen-I from Yeasen Biotechnology Co., LTD. (Shanghai, China; 40136ES10), NLRP3 from Yeasen Biotechnology Co., LTD. (Shanghai, China; 31008ES50), phosphorylated-mothers against decapentaplegic homolog 2 (P-SMAD2) from Wanlei bio Co., LTD. (Shenyang, China; WL02305), P-SMAD3 from Wanlei bio Co., LTD. (Shenyang, China; WL02288), nuclear factor kappa-light-chain-enhancer of activated B cells (NF-KB) from Wanlei bio Co., LTD. (Shenyang, China; WL01273b), SHP2 from Wanlei bio Co., LTD. (Shenyang, China; WL03546), and glyceraldehyde-3-phosphate dehydrogenase (GAPDH) from Wanlei bio Co., LTD. (Shenyang, China; WL01114).

The research team also purchased: (1) a secondary antibody, goat anti-rabbit IgG (H+L) from Wanlei bio Co., LTD. (Shenyang, China; WLa023); (2) transformed C3H mouse kidney-1 (TCMK-1) cells from BFB Co., LTD. (Shanghai, China; BFN608006425); (3) a Western blot kit from Thermo Fisher Scientific Inc. (Shanghai, China; 35055); (4) Tris-buffered saline (TBS) from Yeasen Biotechnology Co., LTD. (Shanghai, China; 60157ES10); (5) dewaxing solution from Yeasen Biotechnology Co., LTD. (Shanghai, China; 60722ES76); (6) antigen retrieval solution from Yeasen Biotechnology Co., LTD. (Shanghai, China; 36319ES60); (7) phosphate buffered saline (PBS) from Yeasen Biotechnology Co., LTD. (Shanghai, China; 60158ES10); (8) optimal cutting temperature (OCT) embedding medium from Yeasen Biotechnology Co., LTD. (Shanghai, China; 36309ES61); (9) normal goat serum from Yeasen Biotechnology Co., LTD. (Shanghai, China; 36119ES10);(10) humidified incubator from Binggu Technology Co., LTD (Shanghai, China; 1AA4510).

The research team also purchased: (1) Tris Buffered Saline with Tween (TBST) from Yeasen Biotechnology Co., LTD. (Shanghai, China; 60145ES76); (2) antibody dilution buffer from Yeasen Biotechnology Co., LTD. (Shanghai, China; 11371ES96); (3) 4',6-diamidino-2-phenylindole (DAPI) working solution from Yeasen Biotechnology Co., LTD. (Shanghai, China; 36308ES20); (4) antifading mounting medium from Yeasen Biotechnology Co., LTD. (Shanghai, China; 36307ES25); (5) fluorescence microscope from OLYMPUS Co., Ltd. (Tokyo, Japan; BX63); (6) cell counting kit-8 (CCK-8) assay from Yeasen Biotechnology Co., LTD. (Shanghai, China; 40203ES76); (7) normal culture medium and Dulbecco's Modified Eagle Medium (DMEM) from Yeasen Biotechnology Co., LTD. (Shanghai, China; 41420ES76); (8) Transwell chambers from Merck KGaA, Darmstadt, Germany (Beijing, China; CLS3422); (10) optical microscope from OLYMPUS Co., Ltd. (Tokyo, Japan; BX53M);

Induction of diabetes, injections of uric acid, and glucose testing. To induce diabetes, the team administered intraperitoneal injections of 50 mg/kg of streptozotocin (STZ) solution to all the C57BL/6J mice at the same time each day, around 1 PM, for 5 consecutive days, carefully ensuring aspiration.

The research team divided 14 mice into two groups, namely STZ modeling + uric acid group (n=7), 0.125-0.5 g/kg intraperitoneal injection of uric acid. The team achieved the most effective modeling at a dose of 0.25g/kg, with blood uric acid levels highest 10 minutes after injection and maintained for more than 4 hours. The other group, the STZ model group (n=7), the control group, did not receive uric acid injection.

The team measured the blood-glucose levels of all the mice using glucose test strips, obtaining the blood from the tail vein and discarding the first drop. If the laboratory mouse blood glucose was ≥16.67 mmol/L or the fasting blood glucose was greater than 11.1 mmol/L, the team considered the modeling to be successful. Mice with successful modeling were anesthetized and euthanized with 20% isoflurane gas, and the kidney tissues were made into paraffin sections for subsequent experiments. All animal experiments followed the 3R principle.

Masson's trichrome staining. The team: (1) for deparaffinization to water, sequentially placed the sections in xylene I for 20 minutes, xylene II for 20 minutes, absolute

ethanol I for 10 minutes, absolute ethanol II for 10 minutes, 95% ethanol for 5 minutes, 90% ethanol for 5 minutes, 80% ethanol for 5 minutes, and 70% ethanol for 5 minutes and then rinsed them with distilled water; (2) for the hematoxylin staining of the cell nuclei, stained the sections with Weigert's iron hematoxylin from the Masson staining kit for 5 minutes, rinsed them with tap water, differentiated them in 1% hydrochloric acid alcohol for a few seconds, rinsed them with tap water, and then rinsed them under running water for several minutes until the blue color returned; (3) for the Ponceau S staining, stained the sections with acid fuchsin solution from the Masson staining kit for 5-10 minutes and rapidly rinsed them with distilled water; (4) for the phosphomolybdic acid treatment, treated the sections with phosphomolybdic acid solution from the Masson staining kit for approximately 3-5 minutes; (5) for the aniline blue staining, directly applied, without prior rinsing, the aniline blue solution from the Masson staining kit for 5 minutes; (6) for differentiation, treated the sections with 1% ice-cold acetic acid for 1 minute; (7) for dehydration and mounting, sequentially placed the sections in 95% ethanol I for 5 minutes, 95% ethanol II for 5 minutes, absolute ethanol I for 5 minutes, absolute ethanol II for 5 minutes, xylene I for 5 minutes, and xylene II for 5 minutes to dehydrate and make them transparent; (8) removed the sections from the xylene, allowed them to air dry briefly, and mounted them with neutral resin; and (9) in the microscopic examination and image-acquisition analysis, collagen fibers, mucin, and cartilage were blue; muscle fibers, cellulose, and red blood cells were red; and cell nuclei were blue-black.

Western blot analysis of NLRP3, ROS Markers, EMT, and SMAD-related protein expression. The research team: (1) extracted cellular total protein using a commercial kit; (2) quantified the protein, separated it by electrophoresis, transferred it to a PVDF membrane, and then blocked it at room temperature for 2 hours; (3) subsequently, incubated the membrane overnight at 4°C with primary antibodies against NLRP3 at 1:2000), P-SMAD2 at 1:2000, P-SMAD3 at 1:2000, and GAPDH at 1:10 000; (4) after washing the membrane, incubated it with the secondary antibody, goat anti-rabbit IgG (H+L) at 1:2000, at 37°C for 90 minutes, followed by visualization; (5) measured the band intensity using Image J software (National Institutes of Health, Bethesda, Maryland, USA) to calculate relative protein expression; (6) repeated the above steps and incubated the membrane with primary antibodies against α-SMA at 1:2000, FN-1 at 1:2000, collagen-I at 1:2000, and GAPDH at 1:10 000, following the same protocol.

In-vitro grouping. For the in-vitro experiment, the research team divided the cells into seven groups. Seven groups of TCMK-1 cells were treated with TGF-β1 (concentration: 2-10 ng/mL): (1) the TGF-β1 group without any other treatments; (2) the TGF-β1 + high glucose group, with the TCMK-1 cells being cultured in a high-glucose medium; (3) the TGF-β1 + high glucose + AGE group, with the TCMK-1 cells being cultured in high-glucose medium and treated with AGE; (4) the TGF-β1 + high glucose + AGE + uric acid group, with the TCMK-1 cells being cultured in a high-glucose medium and treated with AGE and uric-acid crystals; (5) the TGF-β1 + high glucose + SHP2 SiRNA group, with the TCMK-1 cells being treated with SHP2 SiRNA and cultured in high-glucose medium; (6) the TGF-β1 + high glucose + SHP2 SiRNA + AGE group, with the TCMK-1 cells being treated with SHP2 SiRNA, cultured in high-glucose medium, and treated with AGE; and (7) the TGF-β1 + high glucose + SHP2 SiRNA + AGE + uric acid group, with the TCMK-1 cells being treated with SHP2 SiRNA, cultured in high-glucose medium, and treated with AGE and uric acid crystals.

Western blot analysis of NLRP3, ROS markers, SHP2, and other related protein expression. The research team extracted cellular total protein using a commercial Western blot kit. The team: (1) quantified the protein, separated it using electrophoresis, transferred it to a PVDF membrane, and then blocked it at room temperature for 2 hours; (2) subsequently, incubated the membrane overnight at 4°C with primary antibodies against NLRP3 at 1:2000, NF-KB at 1:2000, SHP2 at 1:2000, P-SMAD2 at 1:2000, α-SMA at 1:2000, FN-1 at 1:2000, and GAPDH at 1:10 000; (3) after washing the membrane, incubated it with secondary antibody, goat anti-rabbit IgG, at 1:2000 at 37°C for 90 minutes, followed by visualization; and (4) measured the band intensity using Image J software to calculate the relative protein expression.

Immunofluorescence assay. For each of the seven groups, the research team: (1) for sample pretreatment of the cell samples and washing, removed the culture medium and slowly brought the samples to room temperature, adding Tris-buffered saline (TBS) onto the cells, and rinsed them twice for 5 seconds each time; (2) for fixation, covered the cells with 4% neutral formaldehyde fixative, prepared in TBS, and incubated them at 4°C for 15 minutes, with sufficient fixative being used; (3) for washing, removed the fixative and rinsed three times with pre-chilled TBS buffer at 4°C, each time for 5 minutes; (4) for sample pretreatment and baking for the paraffin-embedded tissue sections, place the paraffin-embedded tissue sections in the same orientation on a slide rack and baked them in a constant-temperature oven at 55°C for 30 minutes; (5) simultaneously placed the dewaxing solution in another container in the same oven at 55°C; (6) for dewaxing to water, transferred the paraffin-embedded tissue sections, together with the slide rack, into the first dewaxing-solution container; (7) took them out together from the oven and let them cool to room temperature for 5 minutes; (8) then immersed the sections in the second dewaxing solution container, followed by sequential immersion in dewaxing solutions 2 and 3, absolute ethanol 1, absolute ethanol 2, and absolute ethanol 3, each for 5 minutes; and (9) rinsed the sections with running water for 5 minutes.

The team: (1) for antigen retrieval in a pressure cooker, added antigen retrieval solution and preheated it on high heat; (2) when the solution reached boiling, placed the tissue

sections in it, ensuring the tissue's complete immersion; (3) covered the cooker, secured the pressure valve, and continued heating it on high heat; (4) after the pressure valve started to rotate and release steam, reduced the heat to medium and started the timer for 2 minutes; (5) then removed the cooker from the heat source and allowed it to depressurize naturally; (6) after the temperature of the retrieval solution reached room temperature, washed the sections three times with PBS, each time for 1 minute; (7) for sample pretreatment, snap-froze the samples in OCT embedding medium; (8) secured the frozen blocks in a tissue chuck and attached it to a cutting assembly; (9) cut the sections to a thickness of 10-20 μm and collected them sequentially; (10) wiped off the excess OCT and outlined the hydrophobic boundaries the tissue using a histology pen;[11] for staining and blocking completely covered the samples with 5% normal goat serum and incubated the slides in a humid chamber at 37°C for 30 minutes; (11) for the cell-culture plates, sealed the plates and incubated them at 37°C in a humidified incubator; (12) The first antibody dilution, according to the instructions to dilute the first antibody dilution buffer; Put in a wet box at 4°C overnight; (13) Add fluorescent secondary antibody: PBST was soaked in the tablet 3 times for 3min each time, absorbent paper was absorbed to dry the excess liquid on the tablet, and then diluted fluorescent secondary antibody was added to the tablet, incubated at 20-37C in a wet box for 1h, and PBST was soaked and sliced 3 times for 3min each time; Note: From the addition of fluorescent secondary antibody, all subsequent steps are carried out in the dark as far as possible; (14) Re-staining of the nucleus: DAPI was added to the sample and incubated for 5 minutes in dark light. The sample was nucleated and washed with PBST 5minx4 times to remove excess DAPI; Use absorbent paper to blot the liquid on the climbing sheet, seal the sheet with a sealing liquid containing anti-fluorescence quench agent, and then observe the acquired images under a fluorescence microscope.

Cell counting kit-8 (CCK-8) assay. Performing the process for all seven groups, the research team: (1) seeded the TCMK-1 cells in a 96-well plate at a density of 2000 cells/100 μl/well and incubated them at 37°C with 5% CO2 in a cell culture incubator; (2) after the cells had completely adhered, place the seven groups of cells in complete culture medium and continued the culturing in the incubator; (3) at 0h, 24h, 48h, and 72h of culture, replaced the medium with serum-free culture medium containing 10% CCK8 reaction solution and incubated the cells for 1 hour before measuring the absorbance (OD) values at a 450 nm wavelength.

Transwell assay. The research team used the Transwell chamber for a cell-migration assay. The team: (1) digested and resuspended the TCMK-1 cells from each group in serum-free culture medium and then seeded them in the upper chamber; (2) seeded a medium containing 10% FBS in the lower chamber as a chemical inducer and cultured the cells under normoxic conditions for 48 hours; (3) removed the nonmigratory TCMK-1 cells on the upper surface using a cotton swab; (4) fixed the TCMK-1 cells on the lower surface with 70% cold ethanol for 1 hour and stained them with 0.5% crystal violet for 20 minutes; and (5) counted the stained cells under an optical microscope in randomly selected fields at 200X.

Figure 1. Comparison of Fibrosis Between the Control Group (N=7), and the STZ Modeling + Uric Acid Group (N=7). Figure 1A shows the fibrosis as assessed using Masson's trichrome staining, and Figure 1B shows the renal fibrosis. $^{**}P < .01$, indicating that the STZ modeling + uric acid group's fibrosis was significantly higher than that of the STZ modeling group

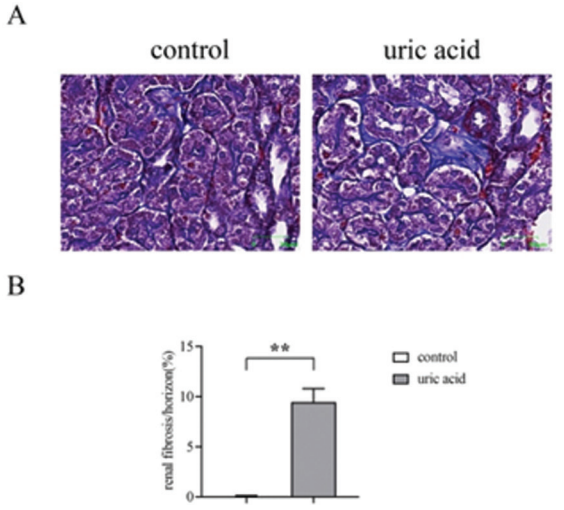

Outcome measures. The research team: (1) using Masson's trichrome staining, examined the fibrosis of renal, tubular epithelial cells in the streptozotocin (STZ) modeling and the STZ modeling + uric-acid groups; (2) used Western Blot analysis to detect the protein expression of NLRP3, "nicotinamide-adenine dinucleotide phosphate (NADPH) oxidase 2" (NOX2), NOX4, α-SMA, FN-1, collagen-I, and SMAD2/3; (3) conducted in-vitro experiments by dividing TCMK-1 cells into different groups: TGF-β1 group, TGF-β1+ high-glucose group, TGF-β1 + high-glucose + AGE group, TGF-β1+ high-glucose + AGE + uric-acid group, TGF-β1+ high glucose + SHP2 small interfering RNA (SiRNA) group, TGF-β1 + high glucose + SHP2 SiRNA + AGE group, and TGF-β1+ high-glucose + SHP2 SiRNA + AGE + uric-acid group for Western Blot experiments; and (4) performed immunofluorescence, CCK-8, and transwell experiments on the seven groups of TCMK-1 cells with different treatments.

RESULTS

Fibroblast Proliferation

The MASSON staining showed that the STZ modeling + uric acid group had more fibrotic cells than the STZ modeling group did (Figure 1A). The STZ modeling + uric acid group's fibrosis was significantly higher than that of the STZ modeling group ($P < .01$). The research team preliminarily concluded that uric acid can accelerate fibrotic progression.

Figure 2. Comparison of the Protein Expression Between the STZ Modeling Group(N=7), and the STZ modeling + Uric Acid Group (N=7). Figure 2A shows the Western blot and protein expression of α-SMA, FN-1, and collagen-I, and Figure 2B shows the Western blot and protein expression of P-SMAD2, P-SMAD3, NLRP3, and ROS-related protein. ***P* < .01, indicating that the STZ modeling + uric acid group's levels of α-SMA, FN-1, collagen-I, P-SMAD2, P-SMAD3, NLRP3, and ROS-related protein were significantly higher than that of the STZ modeling group

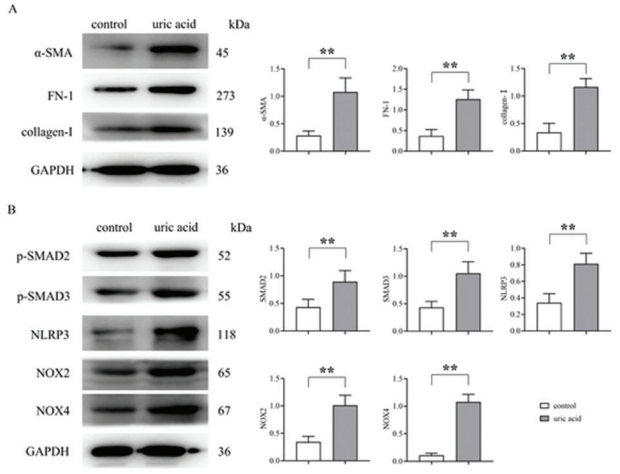

Abbreviations: α-SMA, alpha-smooth muscle actin; FN-1, fibronectin 1; NLRP3, nod-like receptor (NLR) family pyrin domain containing 3; P-SMAD2, phosphorylated-mothers against decapentaplegic homolog 2; P-SMAD3, phosphorylated-mothers against decapentaplegic homolog 3; ROS, reactive oxygen species

Protein Expression: Uric Acid

The Western blots show the STZ modeling + uric acid groups' expression of α-SMA, FN-1, and collagen-I (Figure 2A) and of P-SMAD2, P-SMAD3, NLRP3, and ROS (Figure 2B). The STZ modeling + uric acid group's levels of α-SMA, FN-1, collagen-I, P-SMAD2, P-SMAD3, NLRP3, and ROS-related protein were significantly higher than those of the STZ modeling group (*P* < .01). Since α-SMA, FN-1, and collagen-I are all markers of EMT, the research team observes that high uric acid can promote EMT.

Protein Expression: Combined Factors

A. western blot analysis of the above 7 groups (TGF-β1 group, TGF-β1+ high glucose group, TGF-β1+ high glucose +AGE group, TGF-β1+ high glucose +AGE+ uric acid group, TGF-β1+ high glucose +AGE+ uric acid group). TGF-β1+ high glucose +SHP2 SiRNA group, TGF-β1+ high glucose +SHP2 SiRNA+AGE group, TGF-β1+ high glucose +SHP2 The protein expression of NOX2, NLRP3, NF-KB, SHP2, P-SMAD2, α-SMA and FN-1 in SiRNA+AGE+ uric acid group; B. Statistical analysis of NOX2, NLRP3, NF-KB, SHP2, P-SMAD2, α-SMA, FN-1 protein expression in each group. (Figure 3B).

No significant difference existed in the protein expression levels of NOX2, NLRP3, and NF-KB between the TGF-β1 + high glucose + SHP2 SiRNA, TGF-β1+ high glucose + SHP2 SiRNA + AGE, and TGF-β1 + high glucose + SHP2 SiRNA + AGE + uric acid groups and the TGF-β1+ high glucose, TGF-β1+ high glucose + AGE, and TGF-β1 + high glucose + AGE + uric acid groups, respectively.

Figure 3. Changes of protein expression after treatment with different factors. A. western blot analysis of the above 7 groups (TGF-β1 group, TGF-β1+ high glucose group, TGF-β1+ high glucose +AGE group, TGF-β1+ high glucose +AGE+ uric acid group, TGF-β1+ high glucose +AGE+ uric acid group). TGF-β1+ high glucose +SHP2 SiRNA group, TGF-β1+ high glucose +SHP2 SiRNA+AGE group, TGF-β1+ high glucose +SHP2 The protein expression of NOX2, NLRP3, NF-KB, SHP2, P-SMAD2, α-SMA and FN-1 in SiRNA+AGE+ uric acid group; B. Statistical analysis of NOX2, NLRP3, NF-KB, SHP2, P-SMAD2, α-SMA, FN-1 protein expression in each group. ***P* < .01, indicating that the TGF-β1+ high glucose + SHP2 SiRNA, the TGF-β1+ high glucose + SHP2 SiRNA + AGE, and the TGF-β1 + high glucose + SHP2 SiRNA + AGE + uric acid group's levels of SHP2, P-SMAD2, α-SMA, and FN-1 were significantly lower than those of the TGF-β1 + high glucose, TGF-β1 + high glucose + AGE, and the TGF-β1 + high glucose + AGE + uric acid groups, respectively.

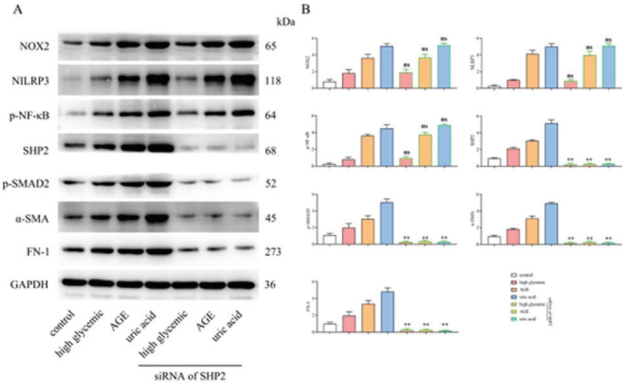

Abbreviations: α-SMA, alpha-smooth muscle actin ; FN-1, fibronectin 1; GAPDH, glyceraldehyde-3-phosphate dehydrogenase; NF-KB, nuclear factor kappa-light-chain-enhancer of activated B cells; NLRP3, nod-like receptor (NLR) family pyrin domain containing 3; NOX2, nicotinamide-adenine dinucleotide phosphate (NADPH) oxidase 2; P-SMAD2, phosphorylated-mothers against decapentaplegic homolog 2; SHP2, Src homology 2 (SH2) domain-containing protein tyrosine phosphatase-2; siRNA, small interfering RNA

The protein expression of SHP2, P-SMAD2, α-SMA, and FN-1 for the TGF-β1 + high glucose + SHP2 SiRNA, the TGF-β1+ high glucose + SHP2 SiRNA + AGE, and the TGF-β1+ high glucose + SHP2 SiRNA + AGE + uric acid groups were significantly lower than those of the TGF-β1 + high glucose,TGF-β1+ high glucose + AGE, and the TGF-β1 + high glucose + AGE + uric acid groups, respectively (*P* < .01).

Overexpression of SHP2

The immunofluorescence showed that the relative fluorescence intensity was low in the TGF-β1 group, moderate in the TGF-β1+ high glucose group, higher in the TGF-β1 + high glucose + AGE group, and highest in the TGF-β1+ high

Figure 4.A. Due to the combination of AGE and uric acid crystals, the relative fluorescence intensity of TGF-β1+ high glucose + AGE + uric acid group was higher than that of TGF-β1 (significant difference), TGF-β1+ high glucose group (significant difference) and TGF-β1+ high glucose + AGE group (difference). The relative fluorescence intensity of TGF-β1+ high glucose + SHP2 SiRNA, TGF-β1+ high glucose + SHP2 SiRNA + AGE, TGF-β1+ high glucose + SHP2 SiRNA + AGE + uric acid groups was significantly lower than that of TGF-β1+ high glucose, TGF-β1+ high glucose + AGE + uric acid groups AGE and TGF-β1+ high glucose + AGE + uric acid groups (**$P < .01$). In terms of OD values expressed by CCK8(FIG. 4b), the cell proliferation of TGF-β1+ high glucose + AGE + uric acid group was stronger than that of TGF-β1 (significant difference), TGF-β1+ high glucose group (significant difference) and TGF-β1+ high glucose + AGE group (difference). B. Cell proliferation in TGF-β1+ high glucose + SHP2 SiRNA, TGF-β1+ high glucose + SHP2 SiRNA + AGE, TGF-β1+ high glucose + SHP2 SiRNA + AGE + uric acid groups was significantly lower than that in TGF-β1+ high glucose, TGF-β1+ high glucose + AGE + uric acid groups AGE and TGF-β1+ high glucose + AGE + uric acid groups (**$P < .01$). C.Due to the combined treatment of AGE and urate crystals, the number of cell migration in TGF-β1+ high glucose + AGE + uric acid group was higher than that in TGF-β1 (significant difference), TGF-β1+ high glucose group (significant difference) and TGF-β1+ high glucose + AGE group (difference). Cell migration in TGF-β1+ high glucose + SHP2 SiRNA, TGF-β1+ high glucose + SHP2 SiRNA + AGE, TGF-β1+ high glucose + SHP2 SiRNA + AGE + uric acid groups was significantly lower than that in TGF-β1+ high glucose, TGF-β1+ high glucose + AGE + uric acid groups AGE and TGF-β1+ high glucose + AGE + uric acid groups (**$P < .01$).

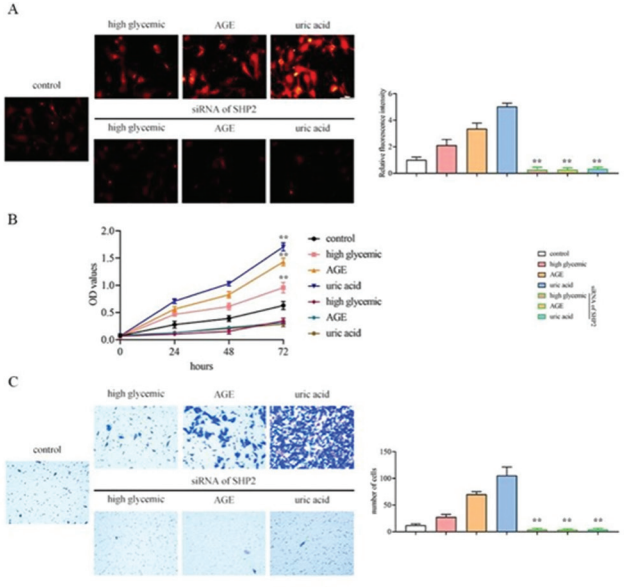

Abbreviations: AGE, advanced glycation end product; CCK8, cell counting kit-8; SHP2, Src homology 2 (SH2) domain-containing protein tyrosine phosphatase-2; siRNA, small interfering RNA

Figure 5. Schematic Diagram of the Mechanism for High Uric Acid Under High-glucose Conditions. High uric acid promotes renal, tubular, epithelial-mesenchymal transition and accelerates the progression of diabetic-nephropathy fibrosis through the activation of the ROS/NLRP3/SHP2 pathway.

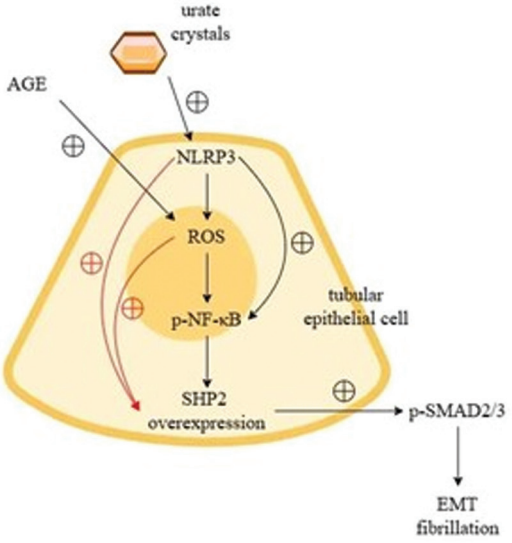

Abbreviations: AGE, advanced glycation end product; EMT, epithelial-mesenchymal transition; NF-KB, nuclear factor kappa-light-chain-enhancer of activated B cells; NLRP3, nod-like receptor (NLR) family pyrin domain containing 3; P-SMAD2, phosphorylated-mothers against decapentaplegic homolog 2; P-SMAD3, phosphorylated-mothers against decapentaplegic homolog 3; ROS, reactive oxygen species; SHP2, Src homology 2 (SH2) domain-containing protein tyrosine phosphatase-2

glucose + AGE + uric acid group (Figure 4A). However, in the TGF-β1 + high glucose + SHP2 SiRNA, TGF-β1+ high glucose + SHP2 SiRNA + AGE, and TGF-β1 + high glucose + SHP2 SiRNA + AGE + uric acid groups, the expression was minimal.

Due to the combination of AGE and uric acid crystals, the relative fluorescence intensity of TGF-β1+ high glucose + AGE + uric acid group was higher than that of TGF-β1 (significant difference), TGF-β1+ high glucose group (significant difference) and TGF-β1+ high glucose + AGE group (difference).

The relative fluorescence intensity of TGF-β1+ high glucose + SHP2 SiRNA, TGF-β1+ high glucose + SHP2 SiRNA + AGE, TGF-β1+ high glucose + SHP2 SiRNA + AGE + uric acid groups was significantly lower than that of TGF-β1+ high glucose, TGF-β1+ high glucose + AGE + uric acid groups AGE and TGF-β1+ high glucose + AGE + uric acid groups ($P < .01$).

In terms of OD values expressed by CCK8(FIG. 4b), the cell proliferation of TGF-β1+ high glucose + AGE + uric acid group was stronger than that of TGF-β1 (significant difference), TGF-β1+ high glucose group (significant difference) and TGF-β1+ high glucose + AGE group (difference).

Cell proliferation in TGF-β1+ high glucose + SHP2 SiRNA, TGF-β1+ high glucose + SHP2 SiRNA + AGE, TGF-β1+ high glucose + SHP2 SiRNA + AGE + uric acid groups was significantly lower than that in TGF-β1+ high glucose,

TGF-β1+ high glucose + AGE + uric acid groups AGE and TGF-β1+ high glucose + AGE + uric acid groups ($P < .01$).

The Transwell assay found that cell proliferation was moderate in the TGF-β1 + high glucose group, higher in the TGF-β1 + high glucose + AGE group, and highest in the TGF-β1 + high glucose + AGE + uric acid group. However, the cell proliferation for the TGF-β1 + high glucose + SHP2 SiRNA, TGF-β1+ high glucose + SHP2 SiRNA + AGE, and TGF-β1 + high glucose + SHP2 SiRNA + AGE + uric acid groups— was minimal (Figure 4C).

Due to the combined treatment of AGE and urate crystals, the number of cell migration in TGF-β1+ high glucose + AGE + uric acid group was higher than that in TGF-β1 (significant difference), TGF-β1+ high glucose group (significant difference) and TGF-β1+ high glucose + AGE group (difference).

Cell migration in TGF-β1+ high glucose + SHP2 SiRNA, TGF-β1+ high glucose + SHP2 SiRNA + AGE, TGF-β1+ high glucose + SHP2 SiRNA + AGE + uric acid groups was significantly lower than that in TGF-β1+ high glucose, TGF-β1+ high glucose + AGE + uric acid groups AGE and TGF-β1+ high glucose + AGE + uric acid groups ($P < .01$).

ROS/NLRP3/SHP2 Pathway

The prior results showed that uric acid crystals can interact with NLRP3 and promote its activity, while AGE can interact with ROS and enhance its activity (Figure 5). NLRP3 acts on ROS, and ROS in turn acts on and promotes P-NF-KB activation. P-NF-KB can interact with SHP2, and overexpression of SHP2 promotes P-SMAD2/3 activation. P-SMAD2/3, in turn, promotes EMT of renal tubular epithelial cells, thereby accelerating the progression of diabetic nephropathy fibrosis.

DISCUSSION

Uric acid salt crystals can act on NLRP3 and promote its activation, while AGEs can act on ROS and enhance its effects. NLRP3 can act on ROS or directly act on NF-κB, and ROS can also act on NF-κB and promote its activation. NF-κB can in turn act on SHP2, and overexpression of SHP2 promotes phosphorylation of SMAD2/3 (P-SMAD2/3).

P-SMAD2/3 can induce EMT in renal tubular epithelial cells, thereby accelerating the progression of diabetic kidney-disease fibrosis. Although fibrosis plays a crucial role in the pathogenesis of diabetic kidney disease, medical practitioners' current understanding of fibrosis associated with diabetic kidney disease remains limited.

Knowledge of the cellular and mechanistic basis of diabetic kidney-disease fibrosis is mainly based on correlational data and extrapolation from concepts derived from other fibrotic conditions. It's necessary not only to study the organ-specific mechanisms of fibrosis in diabetic kidney disease but also to explore the fundamental connections between metabolic disturbances associated with diabetic kidney disease and fibrotic signaling pathways. Clinicians still face numerous challenges in this regard.

Some prior studies suggested the potential regulatory role of SHP2 in the EMT process,[19,20] which the current study confirmed. Overexpression of SHP2 can promote SMAD2/3 phosphorylation, and phosphorylated SMAD2/3 can accelerate the EMT process and promote cellular fibrosis.

CONCLUSIONS

In a high-glucose environment, high uric acid can promote the fibrotic progression of diabetic nephropathy by activating the ROS/NLRP3/SHP2 pathway, leading to mesenchymal transition between renal tubular epithelial cells.

AUTHORS' DISCLOSURE STATEMENT

The authors declared that they have no conflicts of interest related to the study.

AUTHOR CONTRIBUTION

Ling Tian and Qian Yu contributed equally to the work.

REFERENCES

1. Kang DH, Chen W. Uric acid and chronic kidney disease: new understanding of an old problem. *Semin Nephrol*. 2011;31(5):447-452. doi:10.1016/j.semnephrol.2011.08.009
2. Huang R, Fu P, Ma L. Kidney fibrosis: from mechanisms to therapeutic medicines. *Signal Transduct Target Ther*. 2023;8(1):129. doi:10.1038/s41392-023-01379-7
3. Wada J, Makino H. Innate immunity in diabetes and diabetic nephropathy. *Nat Rev Nephrol*. 2016;12(1):13-26. doi:10.1038/nrneph.2015.175
4. Huang R, Fu P, Ma L. Kidney fibrosis: from mechanisms to therapeutic medicines. *Signal Transduct Target Ther*. 2023;8(1):129. doi:10.1038/s41392-023-01379-7
5. van Dam E, van Leeuwen LAG, Dos Santos E, et al. Sugar-Induced Obesity and Insulin Resistance Are Uncoupled from Shortened Survival in Drosophila. *Cell Metab*. 2020;31(4):710-725.e7. doi:10.1016/j.cmet.2020.02.016
6. Tuleta I, Frangogiannis NG. Diabetic fibrosis. *Biochim Biophys Acta Mol Basis Dis*. 2021;1867(4):166044. doi:10.1016/j.bbadis.2020.166044
7. Candido R, Forbes JM, Thomas MC, et al. A breaker of advanced glycation end products attenuates diabetes-induced myocardial structural changes. *Circ Res*. 2003;92(7):785-792. doi:10.1161/01.RES.0000065620.39919.20
8. Forbes JM, Thallas V, Thomas MC, et al. The breakdown of preexisting advanced glycation end products is associated with reduced renal fibrosis in experimental diabetes. *FASEB J*. 2003;17(12):1762-1764. doi:10.1096/fj.02-1102fje
9. Rabbani N, Thornalley PJ. Dicarbonyl stress in cell and tissue dysfunction contributing to ageing and disease. *Biochem Biophys Res Commun*. 2015;458(2):221-226. doi:10.1016/j.bbrc.2015.01.140
10. Berlanga J, Cibrian D, Guillén I, et al. Methylglyoxal administration induces diabetes-like microvascular changes and perturbs the healing process of cutaneous wounds. *Clin Sci (Lond)*. 2005;109(1):83-95. doi:10.1042/CS20050026
11. Riboulet-Chavey A, Pierron A, Durand I, Murdaca J, Giudicelli J, Van Obberghen E. Methylglyoxal impairs the insulin signaling pathways independently of the formation of intracellular reactive oxygen species. *Diabetes*. 2006;55(5):1289-1299. doi:10.2337/db05-0857
12. Dorenkamp M, Nasiry M, Semo D, et al. Pharmacological Targeting of the RAGE-NFκB Signalling Axis Impedes Monocyte Activation under Diabetic Conditions through the Repression of SHP-2 Tyrosine Phosphatase Function. *Cells*. 2023;12(3):513. doi:10.3390/cells12030513
13. Kalluri R, Weinberg RA. The basics of epithelial-mesenchymal transition. *J Clin Invest*. 2009;119(6):1420-1428. doi:10.1172/JCI39104
14. Qu CK, Feng GS. Shp-2 has a positive regulatory role in ES cell differentiation and proliferation. *Oncogene*. 1998;17(4):433-439. doi:10.1038/sj.onc.1201920
15. Wright JH, Drueckes P, Bartoe J, Zhao Z, Shen SH, Krebs EG. A role for the SHP-2 tyrosine phosphatase in nerve growth-induced PC12 cell differentiation. *Mol Biol Cell*. 1997;8(8):1575-1585. doi:10.1091/mbc.8.8.1575
16. Qu CK. Role of the SHP-2 tyrosine phosphatase in cytokine-induced signaling and cellular response. *Biochim Biophys Acta*. 2002;1592(3):297-301. doi:10.1016/S0167-4889(02)00322-1
17. Cunnick JM, Meng S, Ren Y, et al. Regulation of the mitogen-activated protein kinase signaling pathway by SHP2. *J Biol Chem*. 2002;277(11):9498-9504. doi:10.1074/jbc.M110547200
18. Janda E, Lehmann K, Killisch I, et al. Ras and TGF[beta] cooperatively regulate epithelial cell plasticity and metastasis: dissection of Ras signaling pathways. *J Cell Biol*. 2002;156(2):299-313. doi:10.1083/jcb.200109037
19. Oft M, Peli J, Rudaz C, Schwarz H, Beug H, Reichmann E. TGF-beta1 and Ha-Ras collaborate in modulating the phenotypic plasticity and invasiveness of epithelial tumor cells. *Genes Dev*. 1996;10(19):2462-2477. doi:10.1101/gad.10.19.2462
20. Chan RJ, Johnson SA, Li Y, Yoder MC, Feng GS. A definitive role of Shp-2 tyrosine phosphatase in mediating embryonic stem cell differentiation and hematopoiesis. *Blood*. 2003;102(6):2074-2080. doi:10.1182/blood-2003-04-1171